Modelling of the effect of grain boundary diffusion on the oxidation of Ni-Cr alloys at high temperature

Léa Bataillou, Clara Desgranges, Laure Martinelli, Daniel Monceau

Modelling of the effect of grain boundary diffusion on the oxidation of Ni-Cr alloys at high temperature

Léa Bataillou[a,c,*], Clara Desgranges[a,b], Laure Martinelli[a], Daniel Monceau[c]

[a] *Den-Service de la Corrosion et du Comportement des Matériaux dans leur Environnement (SCCME), CEA, Université Paris-Saclay, F-91191, Gif-sur-Yvette, France*
[b] *Safran-Tech, rue des jeunes bois, Châteaufort, CS 80112, 78772 Magny les hameaux, France*
[c] *CIRIMAT, Université de Toulouse, CNRS, INPT, UPS, 4 allée Emile Monso, BP 44362, 33103 Toulouse Cedex 4, France*

Grain boundaries in oxide scales have a strong effect on oxidation kinetics when they act as diffusion short circuits. This study proposes a quantitative evaluation of the phenomenon by modelling. Various cases of oxide microstructure evolution are treated using both analytical and numerical resolutions. Results showed that the effect of oxide grain growth on the oxidation kinetics can be analysed considering a transitory stage for which the oxidation kinetics is not purely parabolic. Some guidelines for choosing the appropriate post-treatment method for the analysis and extrapolation of experimental oxidation kinetics are given.

1. Introduction

Parabolic constants values reported in literature for chromia forming alloys [1–13] are distributed on several orders of magnitude, these values are gathered on Fig. 1. It has been shown that under O_2 atmospheres, chromia grow by diffusion of spieces across the oxide scale [13,15,16] and that diffusion short-circuits, such as grain boundaries in oxide scales, have a major effect on oxidation kinetics [10,17,18].

In his review on the influence of grain boundary diffusion on high temperature oxidation, Atkinson [1] showed that the values of the experimental parabolic constant (k_p) published for chromia are distributed over a range of about three orders of magnitude for the same temperature. Atkinson calculated theoretical k_p values for polycristalline chromia using tracer diffusion coefficient from Hagel *et al.* [14], and k_p value for single cristal chromia using single cristal tracer diffusion coefficient for chromia that he determined experimentally [1]. He showed that experimental reported k_p values were closer to theoretical values corresponding to polycrystalline chromia than to theoretical value corresponding to single crystal chromia. These experimental and theoretical k_p values are plotted on Fig. 1. Knowing that the calculated k_p for polycrystalline chromia can be up to six orders of magnitude higher than the one of single crystal chromia, it was concluded that chromia growth was quantitatively affected by grain boundary diffusion [1]. Notice that such a dispersion of reported k_p values can also be

explained by other phenomena such as a transitory regime caused by formation of NiO [19] or the presence of reactive elements that can slow down diffusion [10,20].

Concerning the influence of grain boundaries, several authors proposed oxidation models taking into account accelerated diffusion by short-circuit diffusion paths. Perrow et al. [18] proposed an analytical solution for oxidation kinetics taking into account grain boundary diffusion in nickel oxide scales. They used the effective diffusion coefficient proposed by Hart [21], which is a weighted average between lattice and short-circuit diffusion coefficients. Hart's law was initially established for the modelling of accelerated diffusion by dislocation. However, it can be adapted to diffusion through grain boundaries. Besides the use of Hart's law, Perrow et al. [18] added the influence of grain size evolution via a parabolic growth law. Hussey et al. [22], who worked on iron oxides growth kinetics, followed the same hypotheses as Perrow et al. [18] and determined an instantaneous parabolic rate constant in the case of a parabolic oxide grain growth. Rhines et al. [23,24] observed cubic oxidation kinetics on NiO scales associated with a cubic grain size growth. Davies and Smeltzer [25,26] proposed an analytical treatment by means of an exponential law for the decay of short-circuit proportion over time. More recently, Hallström et al. [27] proposed a numerical approach based on thermodynamics calculations applied to chromia growth. Nevertheless, this model does not take oxide microstructure evolution into account. Other authors have considered the diffusion through grain boundaries in oxide scales [28–30]
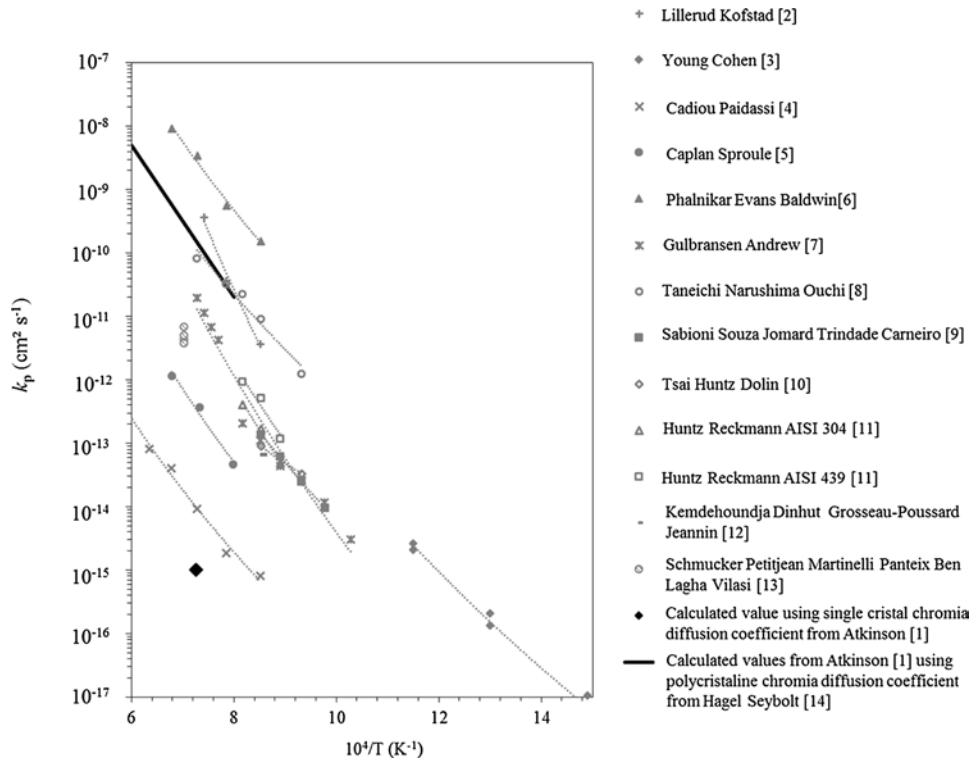

Fig. 1. Arrhenius plot of experimental parabolic rate constant for Cr_2O_3 reported in literature [2–13], and calculated by Atkinson [1] using single crystal or polycrystalline chromia diffusion coefficient from Hagel *et al.* [14].

and even the influence of oxide microstructure on oxidation kinetics [31,32], with an experimental approach.

Some different approaches have been developed concerning oxidation kinetics modelling by taking into account formation and growth of several phases which are also steps forward the description of complex oxide microstructure. Larsson et al. [33] performed a numerical simulation of multiphasic iron oxide growth. Nijdam et al. [34,35] developed coupled thermodynamic-kinetics oxidation model, which is able to predict the phases formed and their impact on oxidation kinetics.

In this framework, this study proposes a new quantitative estimation of the influence of grain boundary diffusion on oxidation kinetics. Oxidation models proposed are applied on chromia-forming alloys. The studied cases consider (1) the evolution of grain size over time, (2) a grain size gradient across the oxide scale, and (3) a combination of both. For the simplest cases (1) and (2), some new analytical solutions were found. However, for the complex cases (3), which combine grain size evolution in time and space, a numerical approach is required. The numerical EKINOX model [36–38] has been used and modified for this study in order to take into account grain boundary diffusion and microstructural evolutions in the oxide scale. Chromia growth kinetics were then modelled using input data based on literature experimental data [10].

The first part of this paper presents the existing oxidation kinetics models available in the literature. These models take into account both lattice and grain boundary diffusion in the oxide scale according to A-type diffusion [39] and consider homogeneous oxide grain size or simple grain size growth law. The second part is dedicated to new analytical models proposed, and to the numerical modelling using the EKINOX code. These new models are able to take into account the oxide grain size growth according to a cubic law and a grain size gradient across the oxide scale. Moreover, a numerical model is adapted in order to treat the complex case of grain size growth and grain size gradient combination.

In results section kinetics obtained using the various analytical and numerical models are presented. Firstly, these oxidation kinetics are

discussed, and then, a parametric study is carried out on the effects of the oxide grain size growth kinetics. In the discussion part, the two methods, which are usually performed for the analysis and the extrapolation of experimental oxidation kinetics, are used on calculated kinetics and they are compared. These are referred in this work as the "parabolic law" method and the "log-log" method. Finally, the two methods are compared for long term extrapolation.

2. Literature models for oxidation kinetics and extrapolation methods

2.1. Wagner's theory simplified

In the case of continuous oxide scale formation, Wagner proposes a model for oxide scale growth that looks at diffusion across the oxide scale as the rate-limiting step [40]. A simplified expression for the parabolic rate constant can be given assuming that the species concentrations at metal/oxide and oxide/gas interfaces are time invariant. This assumption supposes that diffusion occurs through lattice only, that the diffusion coefficient is constant and that usual hypotheses of stationarity, electroneutrality and fluxes conservation are assumed [40]:

$$e^2 = k_{p,L}(t - t_0) + e_0^2 \tag{1}$$

$$k_{p,L} = 2\Omega \widetilde{D}_L \Delta C \tag{2}$$

2.2. Diffusion models taking into account bulk and short-circuit diffusion

When the influence of diffusion along short circuits is taken into account within the global diffusion phenomenon, several limiting cases can be described. These different cases depend on the space distribution of grain size and on the values of diffusion coefficients in lattice and in short circuits [41,42]. Hence three different regimes involving grain boundary diffusion are classically considered and called A-type, B-type
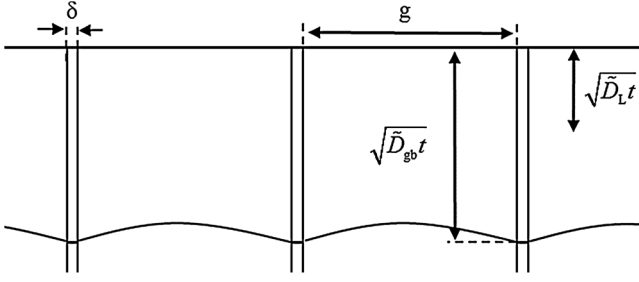
Fig. 2. schematic illustration of diffusion front for A-type diffusion model.

and C-type diffusion. A-type and C-type diffusion represent the two limiting cases of the more general B-type.

In the A-type diffusion model, diffusing atoms are considered to get through lattice and short circuits many times during the studied time period. Therefore, A-type diffusion is often used for long term diffusion, at high temperatures. The diffusion front then corresponds to the mean of paths taken by the diffusing atoms in lattice and short circuits. A schematic illustration of the diffusion front for A-type diffusion is presented in Fig. 2. The diffusion front can be addressed by an effective diffusion coefficient expressed according to Hart's law [21]:

$$\widetilde{D}_{\text{eff}} = \widetilde{D}_{\text{L}}(1 - f) + \widetilde{D}_{\text{gb}}f \tag{3}$$

The parameter f can be expressed as the fraction of short-circuit surface in the material, according to Eq. (4). In the literature, there are other expressions that take into account various grain geometries and surfacic or volumic short-circuit fraction. Eq. (4) corresponds to equiaxed grains and was used by Perrow for high temperature oxidation [18].

$$f = 2\delta/g \tag{4}$$

If grain boundaries are considered as diffusion short circuits, δ corresponds to the grain boundary thickness and g corresponds to the grain size.

Using the A-type diffusion model requires a condition [42]. As diffusing atoms are considered to go through lattice and short circuits several times during the experiment, the typical observation time for this regime must be much longer than the time needed by the atoms to move from a short circuit to another through a lattice region. In other words, the mean free path must be far superior to the short-circuit spacing:

$$2\sqrt{\widetilde{D}_{\text{L}}t} >> g \tag{5}$$

B-type model is effective if the free mean path is the same order of magnitude as the grain size. C-type model is effective for very short times, low temperature, or very high diffusion coefficients in short circuits. The diffusion is assumed to occur almost exclusively through the short-circuit network. The following study looks at A-type diffusion, consequently, B-type and C-type diffusions are not developed.

2.3. Simplified Wagner's theory and effective diffusion coefficient

The effective diffusion coefficient for A regime, as given by Eq. (3), can be combined with the parabolic kinetics coming from Wagner's theory in order to take into account the influence of short-circuit diffusion on oxidation kinetics. Using Eqs. (1) and (3), the oxidation kinetics becomes:

$$e^2 = k_{\text{p,eff}}(t - t_0) + e_0^2 \tag{6}$$

with

$$k_{\text{p,eff}} = 2\Omega\widetilde{D}_{\text{eff}}\Delta C \tag{7}$$

and using (1), (2), (3), (4) and (7) the effective parabolic constant is expressed as follows:

$$k_{\text{p,eff}} = k_{\text{p,L}}\left(1 + \frac{2\delta}{g}\left(\frac{\widetilde{D}_{\text{gb}}}{\widetilde{D}_{\text{L}}} - 1\right)\right) \tag{8}$$

The use of Eq. (6) requires the assumptions involved in Hart's and Wagner's laws, but also the hypothesis that the oxide microstructure is immobilized presenting a uniform and constant grain size. Since microstructure evolutions are common, Perrow et al. [18] proposed a model that takes into account the grain growth over time.

2.4. Perrow's model

Hence, Perrow et al. [18] proposed a more complex oxidation kinetics model for oxide scale growth with the effective diffusion coefficient calculated with Hart's relation (3), but also taking into account the evolution of the grain boundary fraction over time, which is represented by a parabolic grain growth during scale growth:

$$g^2(t) = k_{\text{g}}(t - t_0) + g_0^2 \tag{9}$$

All grains are supposed to be identical in size and follow the same growth kinetics. The oxidation kinetics proposed in Perrow's work [18] contains a calculation error, the exact expression is given below:

$$e^2 - e_0^2 = k_{\text{p,L}}t + \frac{4k_{\text{p,L}}\delta\widetilde{D}_{\text{gb}}}{k_{\text{g}}\widetilde{D}_{\text{L}}}(\sqrt{g_0^2 + k_{\text{g}}t} - g_0) \tag{10}$$

Using the same assumptions as Perrow [18], Hussey et al. [22] proposed an expression of instantaneous growth rate given by Eq. (11). This relation illustrates the fact that the scale growth can be expressed with a parabolic rate constant that evolves over time.

$$k_{\text{p,I}} = 2e\frac{\text{d}e}{\text{d}t} = k_{\text{p,L}}\left(1 + \frac{2\delta\widetilde{D}_{\text{gb}}}{\widetilde{D}_{\text{L}}\sqrt{k_{\text{g}}t + g_0^2}}\right) \tag{11}$$

2.5. Other laws for short-circuit density evolution

2.5.1. Cubic law

Rhines et al. [23,24] proposed a model with a grain volume proportional to time. If the grain volume is considered as the cube of grain size, this is equivalent to a cubic growth law applied to grain size, as expressed in Eq. (12). Rhines noticed that his experimental oxidation kinetics of Ni was in good accordance with a cubic law.

$$g^3(t) = k_{\text{h}}(t - t_0) + g_0^3 \tag{12}$$

However, by using the cubic grain growth law, Rhines did not display the corresponding analytical expression of oxidation kinetics. This point is developed in part II of this study.

2.5.2. Exponential law

Davies and Smeltzer [25,26] modelled the case of inward oxygen diffusion through oxide scale by assuming that the diffusion of oxygen happened through the lattice and an "array" of low resistance paths (diffusion short circuits). They assumed that the proportion of low resistance paths decays according to an exponential law during the oxidation experiment. This model is not discussed or used in this study. Since it was developed for the diffusion through a random array of dislocations, it does not seem adequate for the description of diffusion in oxide grain boundaries.

2.6. Analysis of experimental oxidation kinetics and extrapolation methods

This paragraph focuses on the different methods available in the literature to interpret and extrapolate the experimental oxidation kinetics. These methods usually enable to characterize the experimental oxidation kinetics with an analytical law, and then to extrapolate them over longer time periods.

2.6.1. Parabolic law method

One way to interpret and extrapolate experimental oxidation kinetics curves is to assume that the diffusion phenomenon in the oxide is the main rate limiting step for oxide growth. The oxidation kinetics is thus defined as a parabolic law. However, a purely parabolic law should be applied only in specific cases with the growth of a unique type of oxide, having the same diffusion properties throughout the entire experiment. Most of the time, a transitory regime precedes the establishment of a stationary regime. It is thus necessary to adapt the parabolic law so as to correctly describe the system. Two studies by Pieraggi and Monceau [43,44] propose several parabolic laws designed for different experimental hypotheses. The following mass gain equations have been written for thermogravimetric experiments, however they can be adapted to express oxide thickness. The rate Eq. (13) and kinetic law (14) given below adequately describe oxidation kinetics purely controlled by diffusion. In this case, the initial oxide grown during the transient period ($t < t_i$) has the same protective properties as the oxide growing at $t > t_i$. The apparent growth rate constant can be determined by plotting e^2 or Δm^2 versus t.

$$\frac{d\Delta m}{dt} = \frac{k_p}{2\Delta m} \tag{13}$$

$$\Delta m^2 - \Delta m_i^2 = k_p(t - t_i) \tag{14}$$

The rate Eq. (15) and kinetic law (16) given below also adequately describe oxidation kinetics purely controlled by diffusion. But in this case, the initial oxide growing during the transient period ($t < t_i$) is much less protective than the oxide growing at $t > t_i$. The apparent growth rate constant can be determined by plotting e or Δm versus $t^{1/2}$.

$$\frac{d\Delta m}{dt} = \frac{k_p}{2(\Delta m - \Delta m_i)} \tag{15}$$

$$(\Delta m - \Delta m_i)^2 = k_p(t - t_i) \tag{16}$$

The rate Eq. (17) and the kinetic law (18) given below adequately describe a general oxidation process controlled by a diffusion step characterized by the "k_p" constant and an interfacial reaction step characterized by the "k_l" constant. In this case, the protective properties of the initial oxide are identical to those of the stable oxide.

$$\frac{d\Delta m}{dt} = \frac{1}{(1/k_l) + (2\Delta m/k_p)} \tag{17}$$

$$t - t_i = \frac{\Delta m^2 - \Delta m_i^2}{k_p} + \frac{\Delta m - \Delta m_i}{k_l} \tag{18}$$

The growth rate Eq. (19) and the kinetic law (20) given below adequately describe an overall oxidation process controlled by a diffusion step characterized by the "k_p" constant and an interfacial reaction step characterized by the "k_l" constant. In this case, the initial oxide that grows during the transient period ($t < t_i$) is much less protective than the oxide growing at $t > t_i$. This case is the most general one.

$$\frac{d\Delta m}{dt} = \frac{1}{(1/k_l) + (2(\Delta m - \Delta m_i)/k_p)} \tag{19}$$

$$t - t_i = \frac{(\Delta m - \Delta m_i)^2}{k_p} + \frac{\Delta m - \Delta m_i}{k_l} \tag{20}$$

If none of the equations above (14), (16), (18) or (20) match the entire experimental curve, it is possible to look at k_p as a parameter evolving over time rather than a constant.

This approach has been proposed by Hussey et al. [22]. They calculated the variation of the parabolic rate constant k_p over time using Eq. (21). Later, Atkinson [45] also concluded that the k_p value could change over time particularly when oxide grains grow during the experiment. The k_p value determined using Eq. (21) is sometimes called

"instantaneous k_p" [22,43]. However, this expression must not be used in a general way because it corresponds to the specific case described by Eq. (13).

$$k_{p,I} = 2\Delta m \frac{d\Delta m}{dt} \tag{21}$$

Monceau and Pieraggi [43] have developed a method to calculate k_p value locally that is better adapted to experimental cases. It is based on the local fit of experimental data within a sliding window using the complete parabolic law. Indeed, what is interesting in Eqs. (13)–(20) is that the four rate laws (13), (15), (17), (19) have a common solution in the form of Eq. (20). This means that when the growth of an oxide scale is controlled by diffusion and reaction, even after a transient regime with different oxidation kinetics, then the complete parabolic law (20) can be used to fit the oxidation kinetics. Nevertheless, in order to obtain a good fit, both k_p and k_l should be constant over the fit interval. This last point can be verified by using the complete parabolic law (22) over a sliding time interval over all the experimental data. By using this method, it is then possible to measure the variation of k_p over time and detect the time interval for which k_p is or becomes constant.

$$t = A + B(\Delta m) + C(\Delta m)^2 \tag{22}$$

with

$$k_p = \frac{1}{C} \tag{23}$$

Contrary to Eq. (21), Eq. (22) is compatible with the growth of a first porous, or non-continuous or fast growing transient oxide layer and a second stable and slowly growing oxide, this corresponds to the most general case. When a transitory oxidation regime occurs, the value of k_p changes at the beginning of the oxidation experiment and then stabilizes to a stationary value, corresponding to the stationary regime. The extrapolation procedure consists in identifying of the stationary k_p value and using the kinetic law (22) to extrapolate the mass change kinetics.

This local k_p approach differs from the instantaneous k_p approach presented previously. Indeed, the instantaneous k_p corresponds to the derived kinetics for time t, whereas the local k_p corresponds to a fit of a portion of the oxidation kinetics curve.

2.6.2. Log-log method

If oxidation kinetics cannot be identified at first as a parabolic or a complete parabolic kinetic law, there is another method commonly employed to describe the oxidation kinetics: the "log-log" method. Without assuming any oxidation mechanism (linear, parabolic or cubic laws), the oxidation kinetics is fitted by a power law:

$$(\Delta m - \Delta m_i)^m = k_{\log}t \tag{24}$$

The logarithm of the mass gain (log(Δm)) is then plotted as a function of the logarithm of time according to Eq. (25) in order to extract the values of m and $k_{\log}$ from a linear fit.

$$\log(\Delta m - \Delta m_i) = \frac{1}{m}\log(t) + \frac{1}{m}\log(k_{\log}) \tag{25}$$

The extrapolation for a longer duration is done using Eq. (24).

These two methods, "parabolic law" and "log-log", are discussed in section 5 of this study.

3. Modelling developments for oxidation kinetics

It has been shown here that several analytical models exist to describe oxidation kinetics. Some of them take into account the influence of diffusion by short-circuit paths, and their density evolution over time. The hypotheses made in the oxide microstructure evolution are quite simple. However, complex microstructure have been observed for chromia. For example, Zurek et al. [46] observed various grain sizes

across the oxide scale from nanometric to micrometric scale, and Latu-Romain et al. [16] observed equiaxed grains of hundreds of nanometers size in chromia layer in the inner part of the oxide scale, and columnar grains of hundreds of nanometres length in the layer on the outer part of the oxide scale. In the light of these complex chromia microstructures reported in literature, it seems relevant to take into account more complex grain sizes evolutions in the oxidation kinetics models considering grain size evolution with time and space. Hence, the next part proposes some new original analytical models that take into account different hypotheses on grain size evolution.

3.1. Analytical models

3.1.1. Parabolic oxide grain growth law

First, Perrow's model [18] can be re-considered without the approximation $\widetilde{D}_L(1 - f) \approx \widetilde{D}_L$. Indeed, avoiding this approximation allows extending the use of this model to a wider range of parameter values. The oxidation kinetics given by Perrow (10) can be expressed without the approximation $\widetilde{D}_L(1 - f) \approx \widetilde{D}_L$ and by taking into account initial conditions (e_0, t_0):

$$e^2 = k_{p,L}\left[(t - t_0) + \frac{4\delta}{k_g}\left(\frac{\widetilde{D}_{gb}}{\widetilde{D}_L} - 1\right)\left(\sqrt{k_g t + g_0^2} - \sqrt{k_g t_0 + g_0^2}\right)\right] + e_0^2$$

(26)

Consequently, the expression of the instantaneous parabolic constant (11) becomes:

$$k_{p,I} = 2e\frac{de}{dt} = k_{p,L}\left(1 + \frac{2\delta}{\sqrt{k_g t + g_0^2}}\left(\frac{\widetilde{D}_{gb}}{\widetilde{D}_L} - 1\right)\right)$$

(27)

3.1.2. Cubic oxide grain growth law

By applying the cubic grain growth law according to Eq. (12), the effective diffusion coefficient defined by Eq. (3) can be expressed as follows:

$$\widetilde{D}_{eff} = \widetilde{D}_L\left(1 - \frac{2\delta}{(k_h t + g_0^3)^{1/3}}\right) + \widetilde{D}_{gb}\frac{2\delta}{(k_h t + g_0^3)^{1/3}}$$

(28)

The oxidation kinetics model, assuming a cubic oxide grain growth, can thus be written as follows:

$$e^2 = k_{p,L}\left[(t - t_0) + \frac{3\delta}{k_h}(\frac{\widetilde{D}_{gb}}{\widetilde{D}_L} - 1)[(k_h t + g_0^3)^{2/3} - (k_h t_0 + g_0^3)^{2/3}]\right] + e_0^2$$

(29)

3.1.3. Grain size gradient in the oxide scale

A grain size gradient across the oxide scale is often observed. For example, Zurek et al. [46] studied the chromia scale growth on a Ni-25Cr and observed that the microstructure of the oxide scale presented a variation of grain size across the oxide scale from about 30 nm to 1 μm. Kofstad [28] studied oxidation mechanisms of chromium and also described a chromia grain size difference between the outer part and the inner part of the scale.

Facing this problem, Atkinson [50] used the largest grain size in a NiO scale, grown on pure Ni, to explain the scaling kinetics. But this approximation requires quantitative assessment. It is therefore relevant to take into account the influence of heterogeneous grain sizes in the oxide scale on oxidation kinetics.

Naumenko et al. [32] and Young et al. [47] proposed an oxidation kinetics model for alumina considering a grain size gradient that remains constant over time *i.e.* a grain size proportional to the distance to the oxide gas interface. As the distance to the oxide/gas interface increases over time because of the oxide growth, the global grain size also increases over time. Therefore, in this model, oxide grain size is a
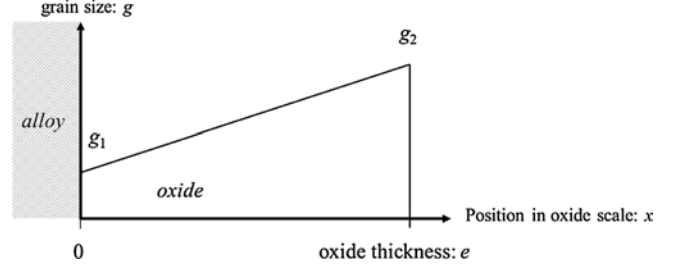

Fig. 3. schematic representation of a linear grain size evolution in the oxide scale.

function of both position in oxide scale and time. According to these works [32,47] such a model is well adapted to alumina growth description. It seems also relevant to be able to uncorrelate grain size evolution over time and across oxide scale for being representative of complex microstructures.

In the present work, a simple case of a uniform grain size gradient with set grain sizes at both alloy/oxide and oxide/gas interfaces is studied. The schematic illustration of the chosen grain size distribution is shown in Fig. 3. The larger grain size is located at the oxide/gas interface and the smaller grain size is located at the metal/oxide interface, as observed by Zurek on Ni-25Cr-Mn alloys at 1000 °C in Ar-20%O_2 [46].

Assuming a grain size gradient across the oxide scale, the effective diffusion coefficient is expressed as follows:

$$\widetilde{D}_{eff} = \widetilde{D}_L\left(1 - \frac{2\delta}{g_1 + \frac{x}{e}(g_2 - g_1)}\right) + \widetilde{D}_{gb}\frac{2\delta}{g_1 + \frac{x}{e}(g_2 - g_1)}$$

(30)

The determination of the oxidation kinetics requires the integration of Eq. (31), using Eq. (30) for the effective chemical diffusion coefficient expression.

$$\frac{de}{dt} = \Omega\widetilde{D}_{eff}\frac{\partial C}{\partial x}$$

(31)

The following change of variable is done:

$$y = \frac{x}{e}$$

(32)

With Eqs. (30) and (32), Eq. (31) becomes:

$$\frac{de}{dt} = \Omega\frac{\Delta C}{e\Delta y}\left[\widetilde{D}_L\left(1 - \frac{2\delta}{g_1 + \frac{x}{e}(g_2 - g_1)}\right) + \widetilde{D}_{gb}\frac{2\delta}{g_1 + \frac{x}{e}(g_2 - g_1)}\right]$$

(33)

By integrating Eq. (33) the following oxide scaling kinetics is obtained for a constant grain size gradient across the oxide scale:

$$e^2 = \frac{k_{p,L}(t - t_0)}{1 + \frac{2\delta(\widetilde{D}_{gb} + \widetilde{D}_L)}{\widetilde{D}_L(g_1 - g_2)}\log\left(\frac{2\delta\widetilde{D}_{gb} + 2\delta\widetilde{D}_L + \widetilde{D}_L g_2}{2\delta\widetilde{D}_{gb} + 2\delta\widetilde{D}_L + \widetilde{D}_L g_1}\right)} + e_0^2$$

(34)

3.1.4. Combination of oxide grain size gradient and grain growth

The case of grain growth with a grain size gradient across the oxide scale corresponds to a variation of grain boundary proportion in both time and space. Such a complex description of oxide scale microstructure and evolution over time is a step further toward a more realistic description of chromia microstructure obtained experimentally. Moreover, the comparison of the oxide scale microstructures obtained after 3 min oxidation and 30 min oxidation indicated a growth of chromia grains over time.

This complex case of oxide microstructure evolution cannot be described with an analytical expression, it is thus treated with the numerical oxidation model EKINOX.

3.2. EKINOX model

EKINOX is a 1D numerical oxidation model. It has been developed to calculate chromia growth kinetics and substrate evolution during high temperature oxidation. Explicit calculations of the concentration of Ni, Cr, O, but also of metallic and oxygen vacancies in the metal/oxide system are carried out by numerical time integration. EKINOX model can thus be useful to understand high temperature oxidation mechanisms. The metal/oxide system is divided into space elements in which fluxes and concentrations are calculated, using Fick's laws according to a finite difference algorithm given in Eqs. (35) and (36). The set of equations that is numerically time integrated has been detailed in previous works [36–38]. The Ni-Cr version has been previously used to calculate the concentration profiles of species and vacancies in the substrate [36–38]. The present work focuses on the oxide scale growth kinetics. The oxide scale is described with two sub-lattices, the cationic sub-lattice containing chromium and chromium vacancies exclusively, and the anionic sub-lattice containing oxygen and oxygen vacancies exclusively. The predominant defects taken here into consideration for lattice diffusion in oxide scale are cationic vacancies, in agreement with experiments carried out by Tsai et al. [10]. In the present study, the effective diffusion coefficient according to Hart's law (3) has been implemented instead of the pure lattice diffusion coefficient, so as to take into account the influence of grain boundaries on oxidation kinetics. This effective diffusion coefficient can vary as a function of time and across the oxide scale. Therefore, the EKINOX numerical model enables to calculate the effects of different grain growth laws and of a grain size gradient. It also allows calculating transitory oxidation regimes. Consequently, the next part shows how EKINOX calculations are used in order to study cases more complex than the ones previously modelled with analytical solutions. In order to validate the numerical resolution, the comparison between numerical calculations and analytical solutions previously mentioned is done (Fig. 4).

$$C_X^n(t + \Delta t) = C_X^n(t) + \frac{J_X^{n-1}(t) - J_X^n(t)}{e^n} \Delta t \tag{35}$$

$$J_X^n(t) = -\widetilde{D}_{\text{eff},X}^n(t) \frac{C_X^{n+1}(t) - C_X^n(t)}{\frac{e^{n+1} + e^n}{2}} \tag{36}$$

3.3. Input data

The input data used for all EKINOX calculations presented here have been chosen in order to represent realistic physical data related to the Ni-30Cr/Cr$_2$O$_3$ system. Input data have been either extracted from published literature or calculated with the Thermocalc software, using Kjellqvist model for chromia description [48]. Most oxidation parameters come from Tsai et al. [10] who performed oxidation and diffusion experiments on Ni-30Cr under 1 atm of O$_2$ at 1173 K. These data are gathered in Table 1.

For analytical calculations, input data are also gathered in Table 1 and $k_{\text{p,L}}$ is determined according to the following relation:

$$k_{\text{p,L}} = 2\widetilde{D}_L \Delta X_V \tag{37}$$

With the parameters chosen for this study, $k_{\text{p,L}} = 8.10^{-15}\,\text{cm}^2\,\text{s}^{-1}$. Relation (37) is identical to relation (2) with:

$$\Delta X_V = \frac{\Delta C}{\Omega} \tag{38}$$

The input data relative to grain growth rate depend on the case studied. All input parameters used to perform the different calculations are summarized in Table 2. For information, the table also gives the corresponding grain size in the oxide at the end of the simulation (300 h oxidation). Cases #P1, #P2, #C1, #C3 lead to unrealistic final grain sizes. These calculations have been performed for a parametric study in order to understand the influence of grain growth on the oxidation kinetics.

For each case, the effective diffusion coefficient is calculated by combining Eqs. (3), (4) and (9) or (12). The effective diffusion coefficients for each case are plotted in Figs. 5–7. When the grain growth is fast, both the proportion of short-circuit diffusion and the effective diffusion coefficient decrease rapidly. As a result, the faster the oxide grain growth the larger slowing effect on the oxidation kinetics.

4. EKINOX results

This section focuses on the results of EKINOX calculations. The first part deals with the validation of the numerical calculations. Oxidation kinetics obtained with EKINOX are compared with the analytical oxidation kinetics represented by Eq. (26), (29) and (34). The second part presents the comparison of several EKINOX kinetics obtained for different types of grain size evolution: case #P4 corresponds to a parabolic grain growth, case #G1 corresponds to a grain size gradient, and case #G1P4 corresponds to a combination of a parabolic grain growth and a grain size gradient. Finally, a parametric study is carried out regarding the influence of k_g and k_h parameters on the oxidation kinetics of different cases: #P1, #P2, #P3 and #C1, #C2, #C3.

4.1. Comparison between EKINOX and analytical models

The initial grain size chosen for the comparison of these different cases is $g_0 = 32\,\text{nm}$. The growth grain constants k_g and k_h are chosen to reproduce the order of magnitude of the average oxide/gas grain size observed experimentally by Tsai et al. [10] after 165 h, which is ~1 μm. k_g and k_h values are respectively $1.67\ 10^{-14}\,\text{cm}^2\,\text{s}^{-1}$ for case #P4 and $1.69\ 10^{-18}\,\text{cm}^3\,\text{s}^{-1}$ for case #C4. For the case assuming a grain size gradient within the oxide scale #G1, the chosen grain sizes are $g_1 = 32\,\text{nm}$ at the metal/oxide interface and $g_2 = 95\,\text{nm}$ at the oxide/gas interface.

These grain sizes were calculated to have a ratio of three between g_1 and g_2, and so that the sum of g_1 and g_2 equals the initial oxide thickness
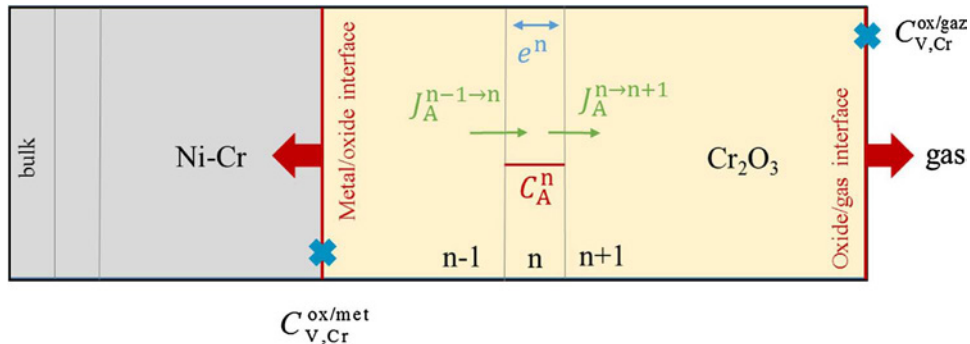

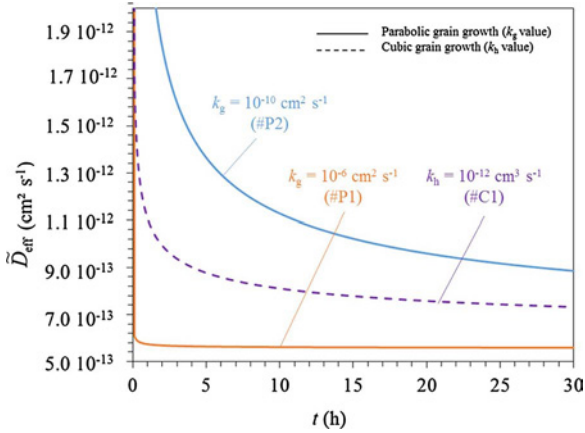**Fig. 4.** Schematic representation of oxide/metal system in EKINOX model.

Table 1
Common EKINOX input data for all simulations.

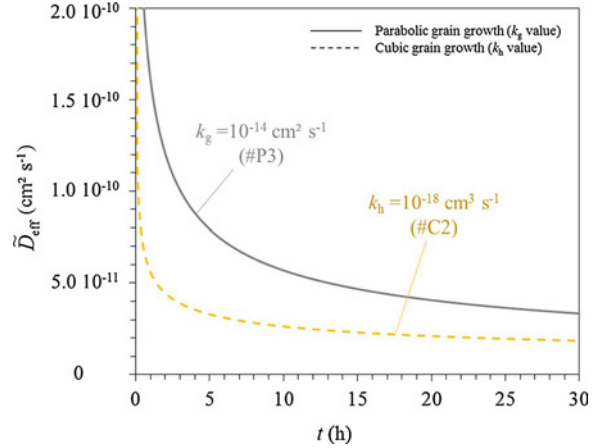| Parameter	Symbol and unit	Value	Origin
Temperature	T (K)	1173	[10]
Alloy composition	X_{Cr}	0.33	[10]
	X_{Ni}	0.67	
Chromium vacancies concentration difference between the oxide/gas and the metal/oxide interface	ΔX_V (atomic fraction in cationic sub-lattice)	$4.62\ 10^{-3}$	Thermocalc calculation [48]
Chromium chemical diffusion coefficient in chromia lattice	$\widetilde{D}_L$ (cm^2 s^{-1})	$5.56\ 10^{-13}$	Adjusted on k_p from [10] with $k_p = 2\widetilde{D}_{eff}\Delta X_V$ and
Chromium chemical diffusion coefficient in chromia grain boundaries	$\widetilde{D}_{gb}$ (cm^2 s^{-1})	$5.56\ 10^{-9}$	$\dfrac{\widetilde{D}_{gb}}{\widetilde{D}_L} = 10^4$
Grain boundary width	δ (nm)	1	[49]
Initial oxide thickness numerically divided into three slabs at t_0	e_0 (µm)	0.127	Calculation choice

Table 2
Input parameters used to perform EKINOX calculations.

Calculation cases	Initial grain size	Type of grain size growth law over time	Parameter k_g (cm^2 s^{-1})	Parameter k_h (cm^3 s^{-1})	Final grain size (t = 300 h)
#P1	$g_0 = 32$ nm	Parabolic Eq. (9)	10^{-6}	–	$g_{300} = 1.04\ 10^4$ µm
#P2	$g_0 = 32$ nm		10^{-10}	–	$g_{300} = 1.04\ 10^2$ µm
#P3	$g_0 = 32$ nm		10^{-14}	–	$g_{300} = 1.04$ µm
#P4	$g_0 = 32$ nm		$1.67\ 10^{-14}$		$g_{300} = 1.34$ µm
#C1	$g_0 = 32$ nm	Cubic Eq. (12)	–	10^{-12}	$g_{300} = 1.03\ 10^2$ µm
#C2	$g_0 = 32$ nm		–	10^{-18}	$g_{300} = 1.03$ µm
#C3	$g_0 = 32$ nm		–	10^{-24}	$g_{300} = 3.23\ 10^{-2}$ µm
#C4	$g_0 = 32$ nm		–	$1.69\ 10^{-18}$	$g_{300} = 1.22$ µm
#G1	$g_1 = 32$ nm	–	–	–	$g_1 = 32$ nm
	$g_2 = 95$ nm				$g_2 = 95$ nm
#G1P4	$g_{1,0} = 32$ nm	Parabolic Eq. (9)	$1.67\ 10^{-14}$	–	$g_{1,300} = 1.34$ µm
	$g_{2,0} = 95$ nm				$g_{2,300} = 1.35$ µm

Fig. 5. effective chemical diffusion coefficient as a function of time for Ni-30Cr oxidized at 1173 K calculated by combining Eqs. (3), (4) and (9) or (12) assuming a parabolic oxide grain growth law for cases #P1 ($k_g = 10^{-6}$ cm^2 s^{-1}) and #P2 ($k_g = 10^{-10}$ cm^2 s^{-1}) and a cubic oxide grain growth for case #C1 ($k_h = 10^{-12}$ cm^3 s^{-1}).

Fig. 6. effective chemical diffusion coefficient as a function of time for Ni-30Cr oxidized at 1173 K calculated by combining Eqs. (3), (4) and (9) or (12) assuming a cubic oxide grain growth for case #C2 ($k_h = 10^{-18}$ cm^3 s^{-1}) and a slow parabolic grain growth for case #P3 ($k_g = 10^{-14}$ cm^2 s^{-1}).

e_0. This corresponds to a bi-layer of grains in the oxide scale.

The comparison between EKINOX results and the analytical models for these three simple cases is presented in Fig. 8. EKINOX results and analytical models are in very good agreement. The small difference is due to the numerical space step chosen for numerical integration and can be reduced with finer space discretization. These results validate the modifications that were made in the EKINOX code. The oxidation kinetics corresponding to the grain size gradient appears very fast and unrealistic compared to chromia growth kinetics usually found in the literature. This is due to the choice of having very small grain sizes at metal/oxide and oxide/gas interfaces which remain unchanged during the calculation process of case #G1. Experimental results from Tsai et al. [10] have been plotted according to a mass gain of 1.5 10^{-4} g cm^{-2} after 8.0 10^4 s, the conversion has been done with a chromia molar mass equal to 152 g mol^{-1} and a density equal to

5.22 g cm^{-3}. The oxide thickness obtained by Tsai et al. [10] after 22 h is in the same order of magnitude as both EKINOX results and analytical kinetics.

4.2. Effect of k_g and k_h values on oxidation kinetics

Oxidation kinetics obtained with Eqs. (26) and (29), corresponding to the different values of k_g and k_h are presented in Figs. 9 and 10. Oxidation kinetics corresponding to the cases #P1, #P2 and #C1 are plotted in the same figure. These cases correspond to a grain size of about 100 µm or more after 300 h. Oxidation kinetics of cases #P3, #C2 and #C3 are plotted in the same figure. These cases correspond to a grain size of about 1 µm or less after 300 h. Oxidation kinetics have been plotted for a time period of 30 h only, indeed, the shape of the
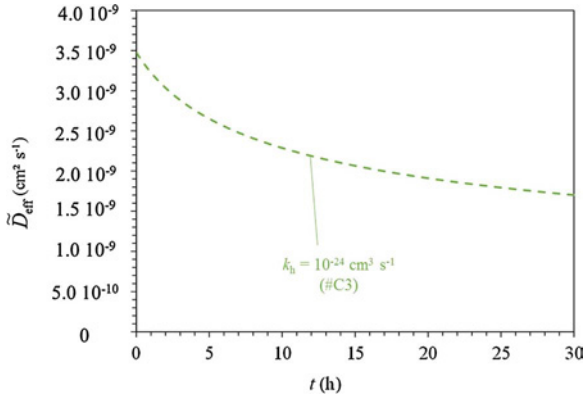
Fig. 7. effective chemical diffusion coefficient as a function of time for Ni-30Cr oxidized at 1173 K calculated by combining Eqs. (3), (4) and (12) assuming a slow cubic grain growth law for case #C3 ($k_h = 10^{-24}$ cm^3 s^{-1}).
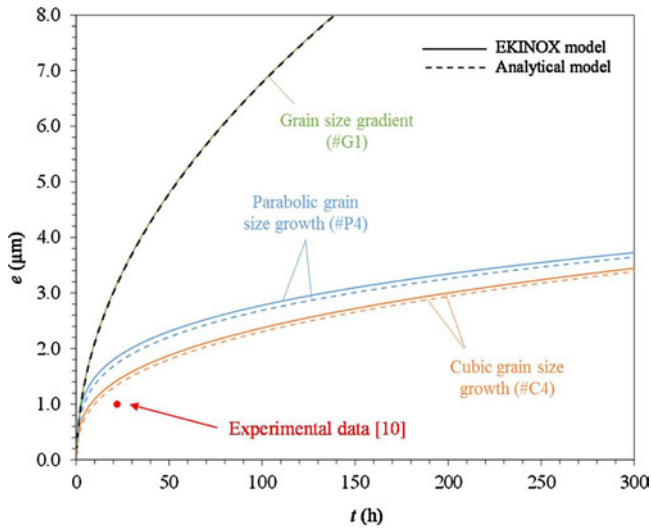

Fig. 8. chromia growth kinetics on Ni-30Cr at 1173 K calculated with EKINOX and analytical models with $g_0 = 32$ nm, and $k_{p,L} = 1.18\,10^{-14}$ cm^2 s^{-1} for different hypotheses: a parabolic grain size growth for case #P4 according to Eq. (9) with $k_g = 1.67\,10^{-14}$ cm^2 s^{-1}, a cubic grain growth law for case #C4 according to Eq. (12) with $k_h = 1.69\,10^{-18}$ cm^3 s^{-1}, and a grain size gradient for case #G1 with $g_1 = 32$ nm and $g_2 = 95$ nm. An experimental data [10] is also displayed.
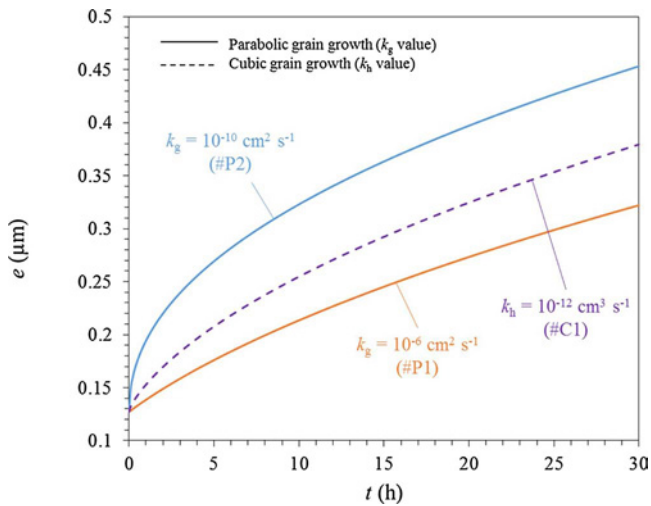

Fig. 9. oxidation kinetics of Ni-30Cr oxidized at 1173 K calculated with Eqs. (26) or (29) assuming a parabolic oxide grain growth law for cases #P1 ($k_g = 10^{-6}$ cm^2 s^{-1}) and #P2 ($k_g = 10^{-10}$ cm^2 s^{-1}) and cubic oxide grain growth for case #C1 ($k_h = 10^{-12}$ cm^3 s^{-1}).
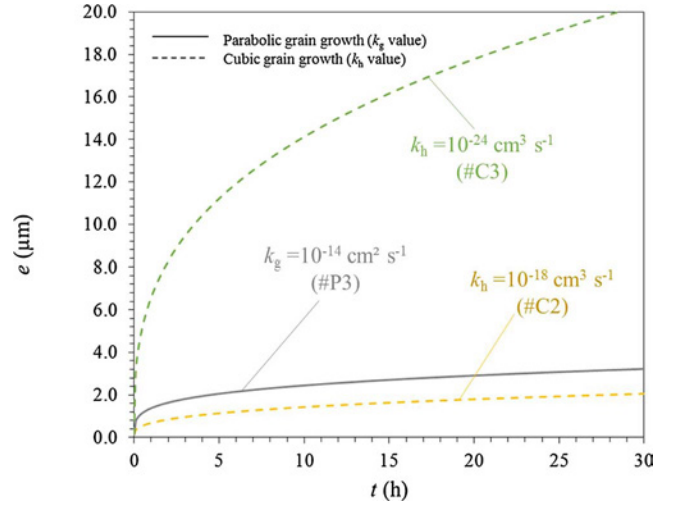

Fig. 10. oxidation kinetics of Ni-30Cr oxidized at 1173 K, calculated with Eqs. (26) and (29) assuming a parabolic grain growth for case #P3 ($k_g = 10^{-14}$ cm^2 s^{-1}) and a cubic grain growth for cases #C2 ($k_h = 10^{-18}$ cm^3 s^{-1}) and #C3 ($k_h = 10^{-24}$ cm^3 s^{-1}).

curves are more visible over short periods of time.

The higher the value of k_g or k_h, the slower the oxidation kinetics. This tendency was expected. It seems interesting however to notice that the general shape of the oxidation curves evolves with the chosen value of k_g or k_h. For cases #P3 and #C3, which have the lowest values of k_g and k_h respectively, oxidation kinetics move away from a parabolic law and appears to be more of a sub-parabolic pattern as shown in Fig. 10. For the highest values of k_g and k_h: 10^{-6} cm^2 s^{-1} and 10^{-12} cm^3 s^{-1} respectively, oxidation kinetics look like a parabolic law as shown in Fig. 9. For the intermediate values of k_g and k_h: 10^{-10} cm^2 s^{-1} and 10^{-18} cm^3 s^{-1} respectively, oxidation kinetics seem to display intermediate shapes as shown in Figs. 9 and 10 respectively.

4.3. Study of the combined effect of grain size gradient within the oxide scale and parabolic grain growth

In this part the three following cases were treated: (1) a parabolic grain growth law for case #P4 according to Eq. (9) with $k_g = 1.67\,10^{-14}$ cm^2 s^{-1}, (2) a grain size gradient for case #G1 with $g_1 = 32$ nm and $g_2 = 95$ nm; and (3) a combination of parabolic grain size growth and grain size gradient for case #G1P4. These different oxidation kinetics are presented in Fig. 11. They are plotted over short oxidation time periods of up to 20 h: this time window corresponds to the interest zone for the simulation parameters chosen.

During the very early stages of oxidation (up to 2 h), the oxide thickness corresponding to a parabolic growth law for case #P4 is higher than the oxide thickness corresponding to the grain size gradient for case #G1. After two hours, this tendency is reversed and the oxide thickness corresponding to the grain size gradient for case #G1 becomes higher than the oxide thickness corresponding to the parabolic grain size growth for case #P4. This result shows that the two oxidation kinetics do not follow the same law. According to Eq. (26), the oxidation kinetics corresponding to a parabolic grain size growth is sub-parabolic, whereas according to Eq. (34), the oxidation kinetics corresponding to a grain size gradient remains purely parabolic.

Concerning case #G1P4, with the combination of parabolic grain size growth and grain size gradient, the oxide thickness is always smaller than that of the two other cases. This result was expected since in this case, the grain size cumulates both growth effects: in time and in space. The proportion of short-circuit diffusion is thus the lowest of the three cases. A similar conclusion can be made for a cubic grain growth law instead of a parabolic grain growth law.

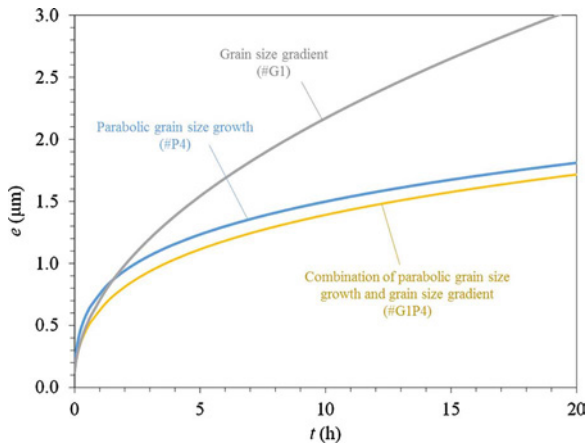Results from this section can be summarized as follows:

Fig. 11. chromia growth kinetics of Ni-30Cr at 1173 K calculated with the EKINOX model corresponding to different hypotheses: a parabolic grain size growth for case #P4 ($k_g = 1.67\,10^{-14}\,\mathrm{cm^2\,s^{-1}}$), a grain size gradient for case #G1 with $g_1 = 32\,\mathrm{nm}$ and $g_2 = 95\,\mathrm{nm}$, and a combination of the parabolic grain size growth and grain size gradient for case #G1P4.
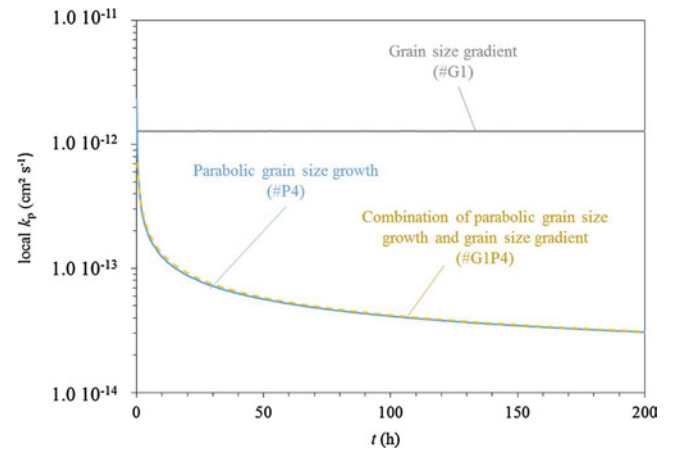

Fig. 12. local k_p from chromia growth kinetics of Ni-30Cr at 1173 K, calculated with the EKINOX model corresponding to a parabolic grain growth for case #P4 ($k_g = 1.67\,10^{-14}\,\mathrm{cm^2\,s^{-1}}$), a grain size gradient for case #G1 with $g_1 = 32\,\mathrm{nm}$ and $g_2 = 95\,\mathrm{nm}$, and a parabolic grain size growth combined with a grain size gradient for case #G1P4.

- A parametric study with analytical calculations showed that k_g and k_h parameters, which characterize the grain growth rate, can have a major influence on the shape of oxidation kinetic curves when considering the grain boundaries as a fast diffusion path.
- EKINOX calculations taking into account the combined effect of grain growth and grain size gradient across the oxide scale for case #G1P4, show that the resulting oxidation kinetics are closer to the oxidation kinetics corresponding to the grain size gradient only for case #P4 for short times, and closer to the oxidation kinetics corresponding to grain growth only for case #G1 for longer times.

Considering these points, it is interesting to discuss post-treatment methods of oxidation kinetics curves as well as derived extrapolations over a longer time range.

5. Discussion

The aim of this discussion is to compare two different methods of interpretation and extrapolation of experimental oxidation kinetics: the "log-log" method and the "parabolic law" method. To do so, the results of the previous calculations are used as if they were experimental data.

5.1. Estimation of the parabolic rate constant values (k_p) from calculated kinetic curves

In this paragraph, oxidation kinetics simulated with EKINOX presented in the previous section are post-treated according to the "parabolic law" method with the local k_p calculation method [43]. This method is presented in Section 2.6.1. The oxidation kinetics considered for the calculation of local k_p values for cases #P4, #G1 and #G1P4 are plotted in Fig. 11. Corresponding local values of k_p are plotted over time in Fig. 12.

The local k_p value corresponding to case #G1 with grain size gradient across the oxide scale but without grain growth is constant. This result could have been predicted as the corresponding kinetics follows a pure parabolic law as determined in Eq. (34). The local k_p value corresponding to the combination of a parabolic grain growth and a grain size gradient for case #G1P4, is close to the local k_p curve corresponding to a parabolic grain growth # P4. These two local k_p curves corresponding to cases with a grain size evolution over time: cases #P4 and #G1P4, decrease rapidly of about one order of magnitude during the first hour of oxidation. It shows that for short time experiments the grain growth can strongly affect the value of the parabolic rate constant determined by a classical fit on the whole kinetic curve. The fact that

the value of k_p changes over time could explain the discrepancy of k_p values found in the literature for different oxidation times as presented in Fig. 1.

5.2. Treatment of oxidation kinetics obtained with EKINOX simulations, using several values for k_g and k_h

5.2.1. Log-log method

The usual way of using the "log-log" method is to perform a linear fit in a log–log plot on the whole kinetic curve. The "log-log" method is explained more extensively on Section 2.6.2. This method overestimates the weight of short times on the global interpretation because of the logarithm function. For long term extrapolation, a more accurate description of oxidation kinetics can be obtained by admitting the existence of a transitory regime for short times. Thus, linear fits are performed on the final portions of the plots, which better describe the stationary regime. In this part, the extrapolation using the "log-log" method is compared to the extrapolation using the "parabolic law" method that also uses the final part of the oxidation kinetic curve. For a fair comparison, this is carried out on the same time interval.

Examples of calculated oxidation kinetics are post-treated with the "log-log" method in Fig. 13 for the parabolic grain growth cases: #P1, #P2, and #P3. Linear fits are performed on a time range from 25 to 30 h. According to the "log-log" method, the parameters m and $k_{\log}$ from Eqs. (24) and (25) can be obtained. These values for the different oxidation kinetics corresponding to the different values of k_g and k_h are gathered in Table 3.

The parameter m reflects the shape of the oxidation kinetics as it corresponds to the value of the time exponent parameter according to Eq. (24). For the fastest grain growth conditions: #P1 with $k_g = 10^{-6}\,\mathrm{cm^2\,s^{-1}}$ and #C1 with $k_h = 10^{-12}\,\mathrm{cm^3\,s^{-1}}$, the m parameter equals 1.4 and 1.7 respectively, that means that the shape of the oxidation kinetics can be bounded between a linear dependence with time and a square root dependence with time. The global oxidation kinetics could thus be interpreted as an over-parabolic law. For the intermediate rate of grain growth with $k_g = 10^{-10}\,\mathrm{cm^2\,s^{-1}}$ and the case with $k_h = 10^{-18}\,\mathrm{cm^3\,s^{-1}}$ corresponding to cases # P2 and #C2 respectively, the m value equals 2.15, and 2.8 respectively, that means that the shape of the oxidation kinetics can be bounded between a square root dependence with time and a cubic root dependence with time. The oxidation kinetic law can be interpreted as parabolic (if m parameter is close to 2) or as an intermediate law between parabolic and cubic. For the slowest grain growth rate: case #P3 with $k_g = 10^{-14}\,\mathrm{cm^2\,s^{-1}}$, the m parameter equals 3.8, that means that the shape of the oxidation
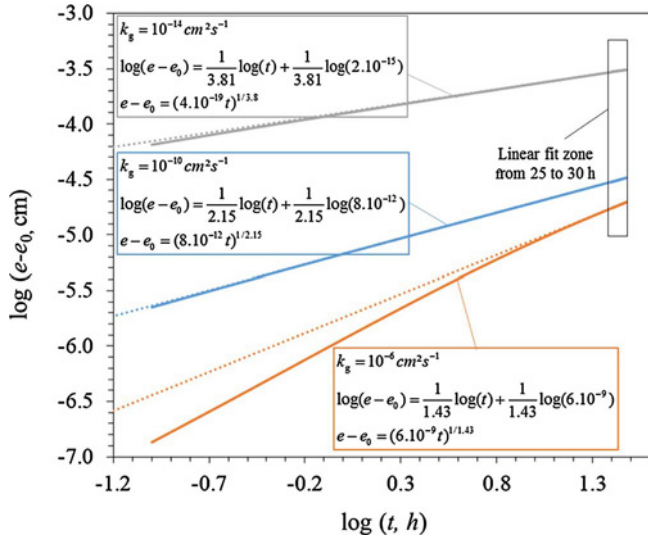
Fig. 13. oxidation kinetics of Ni-30Cr at 1173 K, calculated with Eq. (26), plotted on a log–log scale (e-e_0 (cm), t(s)) assuming a parabolic growth law according to Eq. (9), and for k_g values of $10^{-14}\,cm^2\,s^{-1}$, $10^{-10}\,cm^2\,s^{-1}$ and $10^{-6}\,cm^2\,s^{-1}$. Linear fits are done for the time interval going from 25 to 30 h. Solid lines correspond to calculated kinetics, dotted lines to linear fits.

kinetics can be bounded between a cubic root dependence with time and a fourth root dependence with time. In this case, the oxidation kinetics is close to a quadratic law as the m parameter is close to 4. Finally for the slowest cubic growth rate: case #C3 with $k_h = 10^{-24}\,cm^3\,s^{-1}$, the m parameter equals 3.0, the oxidation kinetic law can be interpreted as cubic, the shape of the oxidation kinetics can be approximated by a cubic root dependence with time. This last particular case matches Rhines' observations [23,24] with a cubic grain growth law associated with a cubic oxidation kinetics. The grain size is thus proportional to the oxide thickness.

By using the "log-log" method, oxidation kinetics could be plotted with an over-parabolic, cubic or quadratic law despite the fact that growth mechanisms remain identical (only kinetic constants change).

These results can be explained by means of the analytical oxidation models presented in part II of this work: Eq. (26) for a parabolic oxide grain growth and Eq. (29) for a cubic oxide grain growth. The oxidation kinetic law given by Eq. (26) is composed of three terms. One term proportional to time, one term proportional to the square root of time, and one constant term. Depending on the values of the parameters of the law, one term of the kinetic law can become predominant compared to the others for a given time range, and the global oxidation kinetics follows the tendency given by the predominant term. If the predominant term is the one proportional to time, the global oxidation

kinetics has a parabolic pattern, for example #P1 with $k_g = 10^{-6}\,cm^2\,s^{-1}$. If the predominant term is the one proportional to the square root of time, the global oxidation kinetics has a quadratic pattern, for example #P3 with $k_g = 10^{-14}\,cm^2\,s^{-1}$. Transition values of k_g and k_h from one type of law to the other can be determined for a given duration of the experiment. This calculation is described in Appendix B.

Some oxide thickness extrapolations from 30 h oxidation kinetics can be calculated according to kinetic laws using Eq. (24) with the data gathered in Table 3. The corresponding extrapolated oxide thickness for 1 year and 10 years of oxidation are gathered in Table 3. For comparison, real thicknesses from analytical laws (26) and (29) are also reported. Relative errors in the extrapolation range from 0.1% to 217%. The gap between extrapolated and analytical values increases with longer extrapolation times and with the values of k_g and k_h. Indeed, the relative error is the highest for cases #P1 and #C1, which correspond respectively to the highest values of k_g and k_h.

5.2.2. Complete parabolic law method

Another post-treatment method applied to kinetic curves has been carried out by using Eq. (22), which corresponds to the complete parabolic law. This law has been adjusted to fit the curves on the same time interval as determined previously (for the "log-log" method): from 25 to 30 h. $k_{p,(25h)}$, values obtained following these adjustments are listed in Table 3.

$k_{p,(25h)}$ values given in Table 3 and obtained in the 25–30 h time period are higher for cases with the lowest values of k_g and k_h. As grain size increases continuously over time, the local k_p value decreases over time, and for a long enough time, the second part of Eqs. (26) and (29) become negligible compared to the first part of the relations. The $k_{p,stat}$ value is expected to reach $k_{p,L} = 8.10^{-15}\,cm^2\,s^{-1}$ for an infinite time. A similar observation can be made on the values of the effective diffusion coefficient plotted in Figs. 5–7, which decrease over time with the grain growth. The effective diffusion coefficients are obviously expected to reach the lattice diffusion coefficient for an infinite time. In the cases studied here, the time needed to reach this stationary regime depends on grain growth kinetics, and is thus linked to the values of k_g and k_h. If the grain growth is fast, the effective diffusion coefficient quickly reaches its stationary value. In contrast, if the grain growth is slow, the effective diffusion coefficient reaches its stationary value after a long time.

The $k_{p,(25h)}$ values obtained by parabolic fit gathered in Table 3 for cases #P1, #P2 and #C1 are of the same order of magnitude as $k_{p,L} = 8.10^{-15}\,cm^2\,s^{-1}$. It can thus be assumed that, in these cases, the stationary regime is reached after 25 h. For cases #P3, #C2 and #C3 however, the local k_p value is different from the $k_{p,L}$ value, ranging from one to three orders of magnitude. This is due to the fact that the stationary regime has not been reached after 25 h. The k_p values obtained

Table 3

Analytical oxide thickness calculated with Eqs. (26) and (29) respectively for parabolic grain growth #P1, #P2, #P3 and cubic grain growth #C1, #C2, #C3. m, k_{log}, and $k_{p,(25h)}$ parameters are obtained from extrapolations of analytical oxidation kinetics of Ni-30Cr on 30 h at 1173 K according to "log-log" and "parabolic law" methods. Extrapolated oxide thicknesses corresponding to "log-log" and "parabolic law" extrapolation methods according to Eqs. (24) and (22) and calculated with parameters m, k_{log} and $k_{g,(25h)}$ are given for 1 year and 10 years. Finally, relative errors on oxide thickness between analytical and extrapolated values are given.

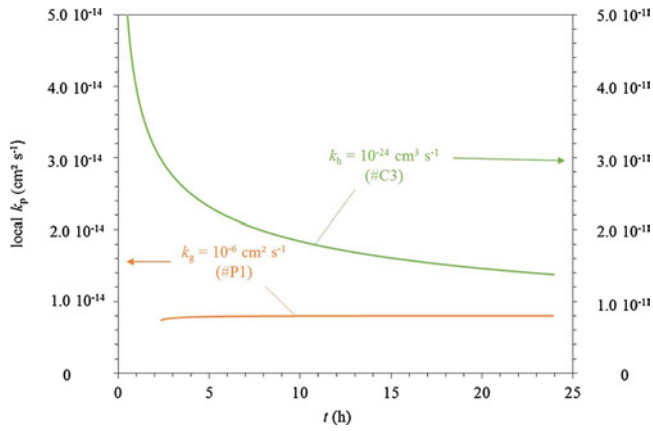| Calculation case	Oxide grain growth parameter		Analytical oxide thickness (µm)		log–log method						Parabolic law method				
					m	k_{log}	$e_{log\text{-}log}$ (µm)		Relative error on oxide thickness (%)		$k_{p,(25h)} = 1/C$ $(cm^2\,s^{-1})$	$e_{parablaw}$ (µm)		Relative error on oxide thickness (%)	
			1 year	10 years			1 year	10 years	1 year	10 years		1 year	10 years	1 year	10 years
#P1	k_g	10^{-6}	5.0	15.9	1.4	2.10^{-12}	10.2	50.4	104	217	8.10^{-15}	4.9	15.8	2	0.6
#P2	$(cm^2\,s^{-1})$	10^{-10}	5.2	16.1	2.15	4.10^{-15}	4.8	14.3	8	11	8.10^{-15}	5.1	16.0	2	0.6
#P3		10^{-14}	14.2	28.4	3.8	4.10^{-19}	13.8	25.2	3	11	8.10^{-14}	18.0	51.7	27	82
#C1	k_h	10^{-12}	5.2	16.2	1.7	2.10^{-13}	7.6	29.6	46	83	9.10^{-15}	5.3	16.5	2	2
#C2	$(cm^3\,s^{-1})$	10^{-18}	14.4	33.1	2.8	4.10^{-16}	14.8	33.7	3	2	9.10^{-14}	18.2	54.6	21	67
#C3		10^{-24}	135.1	291.3	3.0	9.10^{-14}	135.0	292.2	0.1	0.3	8.10^{-12}	177.4	529.6	31	82

Fig. 14. local k_p value corresponding to the oxidation kinetics of Ni-30Cr at 1173 K, calculated with Eqs. (26) and (29), corresponding respectively to $k_g = 10^{-6}\,\text{cm}^2\,\text{s}^{-1}$ for case #P1 (scale on the left) and $k_h = 10^{-24}\,\text{cm}^3\,\text{s}^{-1}$ for case #C3 (scale on the right).

by parabolic fit for these three cases thus do not correspond to the stationary k_p value. Consequently the parabolic extrapolation is not correct and should not be employed in these cases. The evolution of local k_p values of cases #P1 and #C3 are plotted in Fig. 14. In case #P1, local k_p is stationary throughout the entire time range chosen, whereas in case #C3, the value of k_p decreases dramatically at early oxidation times and is still decreasing at the end of the experiment. This illustrates that the stationary value of k_p has not been reached at the end of the oxidation time chosen here.

The oxide thickness can be extrapolated using complete parabolic laws with Eq. (22) and parameters given in Table 3. This same table displays the values of these extrapolated oxide thicknesses for 1 year and 10 years, and the corresponding analytical values calculated with Eqs. (26) and (29). The relative errors between extrapolated and analytical values range from 0.6% and 82%. Contrary to the extrapolations obtained with the "log-log" method, discrepancies increase as values of k_g or k_h decrease. Indeed, the most important relative errors are found for cases #P3, #C2 and #C3, those with the slowest grain growth rate, and therefore having the longest transient stage of oxidation. For the slowest grain growth rates, the oxidation kinetics is far from the parabolic regime, even over a long time range. As shown in Fig. 14 with case #C3, local k_p had still not reached its stationary value after 25 h.

To conclude this part, the best way to fit the experimental data is to use the local k_p method first, in order to determine if the parabolic stationary regime is reached. If so, the best extrapolation is given by the complete parabolic law using the value of k_p obtained for the stationary regime, *i.e.* $k_{p,\text{stat}}$. This method is more accurate than the one that uses a power law, even if this latter has been obtained by a fit over longer oxidation times. If no parabolic stationary regime can be determined for the local k_p curve, as is the case for very slow grain growth rates, it can be then more appropriate to use the "log-log" method for extrapolation.

However, when possible, the best method is to perform a longer experiment until the stationary regime is reached, and to extrapolate with the "parabolic law" method using the stationary k_p and the complete law. The alternative method consists in using an analytical or numerical model that includes grain growth kinetics, if the evolution of local k_p is assumed to be due to the oxide grain size evolution.

6. Conclusion

The conclusions that can be drawn from this work are the following:

1) Grain boundary diffusion and oxide scale microstructure evolution over time should be considered to interpret oxidation kinetics which are not purely parabolic.
2) Analytical models are presented considering a cubic grain growth law and a grain size gradient across the oxide scale. A numerical resolution, using for example the EKINOX model, can be used to simulate more complex cases of combination of grain size growth and grain size gradient but also other grain size growth laws.
3) Calculation results show that even when using the same oxide growth mechanism, *i.e.* control by faster diffusion in the oxide due to grain boundaries diffusion, the evolution rate of diffusion short-circuit proportion over time modifies the oxide growth kinetics, and even their global shapes.
4) Depending on grain growth kinetics, the experimental oxidation kinetics that derive from a mixed diffusion phenomenon in bulk and in grain boundaries can be globally interpreted with various laws from over-parabolic to parabolic, sub-parabolic, cubic and even quadratic.
5) Extrapolation of oxidation kinetics can be strongly affected by the choice of the method, and also by the duration of the oxidation experiment. The use of the "local k_p" helps identifying if the parabolic stationary regime is reached and thus helps performing accurate extrapolations of oxidation kinetics. If the stationary regime is not reached during the oxidation time of the experiment, no extrapolation should be done. If longer experiment cannot be performed, extrapolation using the "log-log" method might be a better choice. However, experimenters have to keep in mind that this extrapolation is not based on clearly identified rate controlling phenomena and then should be used with caution.

This study focuses on the growth of chromia, however, similar conclusions can be drawn on the growth of other oxides.

Acknowledgments

Appendix A. Symbols used

A, B, C: coefficients used for the "complete parabolic law fit" (respectively in s, s cm^{-1}, s cm^{-2})
X_A^n: atomic site fraction of A in the slab n in the EKINOX model
X_A: atomic site fraction of A (A = Cr or Ni) in alloy
C_X^n: site fraction for specie X calculated on EKINOX model in slab n (dimensionless)
$\widetilde{D}_{\text{eff}}$: effective chemical diffusion coefficient (cm^2 s^{-1})
$\widetilde{D}_{\text{gb}}$: grain boundary chemical diffusion coefficient (cm^2 s^{-1})
$\widetilde{D}_{\text{L}}$: chemical diffusion coefficient in oxide lattice (cm^2 s^{-1})
J_X^n: flux of specie X calculated on EKINOX model in slab n (site m^{-2} s^{-1})
e: oxide scale thickness, e_0 corresponds to oxide thickness at initial time t_0 (cm)
f: atomic site fraction on short-circuits path per unit area (dimensionless)
g: grain size, g_0 grain size at initial time t_0, g_1 corresponds to oxide grain size at metal/oxide interface, g_2 corresponds to oxide grain size at oxide/gas interface (cm)

k_g: parabolic coefficient for the grain growth law ($cm^2 s^{-1}$)

k_h: cubic coefficient for the grain growth law ($cm^3 s^{-1}$)

k_l: linear constant of the oxide scale growth ($cm s^{-1}$) or ($g cm^{-2} s^{-1}$)

k_{log}: kinetic parameter used for the power law kinetics of oxide scale growth ("log-log" method) (units depend on exponent of the power law: m)

k_p: parabolic constant of the oxide scale growth, $k_{p,eff}$ corresponds to effective parabolic constant in case of diffusion through lattice and grain boundaries, $k_{p,I}$ corresponds to instantaneous parabolic constant of the oxide scale growth, $k_{p,L}$ corresponds to parabolic constant of the oxide scale growth in case of diffusion through lattice only, $k_{p,stat}$ corresponds to local parabolic constant corresponding to the stationary regime of the oxide scale growth ($cm^2 s^{-1}$) or ($g^2 cm^{-4} s^{-1}$)

m: exponent used for the power law kinetics of oxide scale growth ("log-log" method) (dimensionless)

t: time, t_0 corresponds to initial time (s) or (h)

x: position in the oxide scale (cm)

δ: short-circuit thickness, or grain boundary thickness (cm)

ΔC: difference in defect concentration between the oxide/gas interface and the metal/oxide interface ($atom\,cm^{-3}$)

Δm: mass gain per unit area, Δm_i corresponds to initial mass gain per unit area ($g cm^{-2}$)

ΔX_V: difference between vacancy site fraction at oxide/gas and metal/oxide interfaces (dimensionless)

Δy: difference of relative position in oxide scale (dimensionless)

Ω: volume of oxide per oxide site ($cm^3 atom^{-1}$)

Appendix B. Calculation of transition k_g and k_h values

With an oxidation time of 30 h, a transition k_g value, so called k_g^{tr} can be determined for transition between predominance of the square root part of time. Right side of Eq. (26) and predominance of the linear part of time *i.e.* left side of Eq. (26).

$$k_{p,L}t + e_0^2 = \frac{4\delta k_{p,L}}{\sqrt{k_g^{tr}}}\left(\frac{\widetilde{D}_{gb}}{\widetilde{D}_L} - 1\right)\sqrt{t} \tag{39}$$

leading to:

$$k_g^{tr}=\left(\frac{4\delta k_{p,L}}{k_{p,L}\sqrt{t} + \frac{e_0^2}{\sqrt{t}}}\left(\frac{\widetilde{D}_{gb}}{\widetilde{D}_L} - 1\right)\right)^2 \tag{40}$$

Following the same approach, the transition value of the cubic growth rate of grain size k_h^{tr} leading to different regimes of oxidation kinetics can be determined:

$$k_h^{tr} = \left(\frac{3\delta k_{p,L}}{k_{p,L}t^{1/3} + \frac{e_0^2}{t^{2/3}}}\left(\frac{\widetilde{D}_{gb}}{\widetilde{D}_L} - 1\right)\right)^3 \tag{41}$$

By using the parameters chosen in this study for case #P2, with $k_g = 10^{-10}\,cm^2 s^{-1}$, global oxidation kinetics have a mixed parabolic and quadratic tendency. For parameters corresponding to case #C2, with $k_h = 10^{-18}\,cm^3 s^{-1}$, oxidation kinetics have a mixed parabolic and cubic tendency.

In order to have the time proportionate term predominant in Eq. (26), the value of k_g value must respect the condition: $k_g >> k_g^{tr}$, this corresponds to case #P1, with $k_g = 10^{-6}\,cm^2 s^{-1}$. By using a similar approach for a cubic oxide grain growth law, the condition $k_h >> k_h^{tr}$ corresponds to case #C1, with $k_h = 10^{-12}\,cm^3 s^{-1}$. These cases lead to oxidation kinetics following a parabolic law.

In order to have the term proportional to the square root of time predominant in Eq. (26), the value of k_g must respect the condition: $k_g << k_g^{tr}$, this corresponds to case #P3, with $k_g = 10^{-14}\,cm^2 s^{-1}$. By using a similar approach for a cubic oxide grain growth law, the condition $k_h >> k_h^{tr}$ corresponds to case #C3, with $k_h = 10^{-24}\,cm^3 s^{-1}$. These cases lead to oxidation kinetics following a quadratic and a cubic law respectively.

Data availability

The processed data (output of EKINOX code) required to reproduce these findings, which are oxide thicknesses over time, and effective diffusion coefficient, are already shared in graphs in Figs. 8 and 11.

References

[1] A. Atkinson, R.I. Taylor, G. Simkovich, V.S. Stubican (Eds.), Transport in Nonstoichiometric Compounds, vol. 129, 1985, pp. 285–295.
[2] K.P. Lillerud, P. Kofstad, J. Electrochem. Soc. 127 (1980) 2410–2419.
[3] D.J. Young, M. Cohen, J. Electrochem. Soc. 124 (1977) 769–774.
[4] L. Cadiou, J. Paidassi, Mem. Scient. De La Revue De Metall. 66 (3) (1969) 217–225.
[5] D. Caplan, G.I. Sproule, Oxid. Met. 9 (5) (1975) 459–472.
[6] C.A. Phalnikar, E.B. Evans, W.M. Baldwin, J. Electrochem. Soc. 103 (1956) 429–438.
[7] E.A. Gulbransen, K.F. Andrew, J. Electrochem. Soc. 99 (10) (1952) 402–406.
[8] K. Taneichi, T. Narushima, Y. Iguchi, C. Ouchi, Materi. Trans. 47 (10) (2006) 2540–2546.
[9] A.C.S. Sabioni, J.N.V. Souza, V. Ji, F. Jomard, V.B. Trindade, J.F. Carneiro, Solid State Ionics 276 (2015) 1–8.
[10] S.C. Tsai, A.M. Huntz, C. Dolin, Mater. Sci. Eng. A 212 (1996) 6–13.
[11] A.M. Huntz, A. Reckmann, C. Haut, C. Sévérac, M. Herbst, F.C.T. Resende, A.C.S. Sabioni, Mater. Sci. Eng. A 447 (1–2) (2007) 266–276.
[12] M. Kemdehoundja, J.F. Dinhut, J.L. Grosseau-Poussard, M. Jeannin, Mater. Sci. Eng. A435 (2006) 666–671.
[13] E. Schmucker, C. Petitjean, L. Martinelli, P.J. Panteix, S. Ben Lagha, M. Vilasi, Corros. Sci. 111 (2016) 474–485.
[14] W.C. Hagel, A.U. Seybolt, J. Electrochem. Soc. 108 (12) (1961) 1146–1152.
[15] G.M. Ecer, G.M. Meier, Oxid. Met. 13 (2) (1979) 119–158.
[16] L. Latu-Romain, Y. Parsa, S. Mathieu, M. Vilasi, A. Galerie, Y. Wouters, Corros. Sci. 126 (2017) 238–246.
[17] R.E. Lobnig, H.P. Schmidt, K. Hennesen, H.J. Grabke, Oxid. Met. 37 (1/2) (1992) 81–93.
[18] J.M. Perrow, W.W. Smeltzer, J.D. Embury, Acta Metall. 16 (1968) 1209–1218.
[19] E. Essuman, G.H. Meier, J. Zurek, M. Hansel, T. Norby, L. Singheiser, W.Q. Quadakkers, Corros. Sci. 50 (2008) 1753–1760.

[20] K. Przybylski, G.J. Yurek, J. Electrochem. Soc. 135 (2) (1988) 517–523.
[21] E.W. Hart, Acta Metall. 5 (1957) 595.
[22] R.J. Hussey, G.I. Sproule, D. Caplan, M.J. Graham, Oxid. Met. 11 (2) (1977) 65–79.
[23] F.N. Rhines, R.G. Connell Jr., J. Electrochem. Soc. 124 (1977) 93–105.
[24] F.N. Rhines, R.G. Connell Jr., M.S. Choi, J. Electrochem. Soc. 126 (6) (1979) 1061–1066.
[25] D.E. Davies, U.R. Evans, J.N. Agar, Proc. Roy. Soc. A225 (1954) 443–462.
[26] W.W. Smeltzer, R.R. Haering, J.S. Kirkaldy, Acta Metall. 9 (1961) 880–885.
[27] S. Hallström, M. Halvarsson, L. Höglund, T. Jonsson, J. Agren, Solid State Ionics 240 (2013) 41–50.
[28] P. Kofstad, K.P. Lillerud, J. Electrochem. Soc. 127 (11) (1980) 2410–2419.
[29] M.W. Barsoum, J. Electrochem. Soc. 148 (2001) C544–C550.
[30] J.L. Smialek, Corros. Sci. 91 (2015) 281–286.
[31] R. Peraldi, D. Monceau, B. Pieraggi, Oxid. Met. 58 (2002) 249–273.
[32] D. Naumenko, B. Gleeson, E. Wessel, L. Singheiser, W.J. Quadakkers, Metall. Mater. Trans. A 38A (2007) 2974–2983.
[33] H. Larsson, T. Jonsson, R. Naraghi, Y. Gong, R.C. Reed, J. Agren, Mater. Corros. 68 (2) (2017) 133–142.
[34] T.J. Nijdam, W.G. Sloof, Acta Mater. 55 (2007) 5980–5987.
[35] T.J. Nijdam, L.P.H. Jeurgens, W.G. Sloof, Acta Mater. 51 (2007) 5295–5307.
[36] C. Desgranges, N. Bertrand, K. Abbas, D. Monceau, D. Poquillon, et al., P. Steinmetz (Ed.), High Temperature Corrosion and Protection of Materials 6, Prt 1 and 2, Proceedings, Trans Tech Publications Ltd, 2004, pp. 481–488 461–464.
[37] N. Bertrand, C. Desgranges, M. Nastar, G. Girardin, D. Poquillon, D. Monceau,
P. Steinmetz, I.G. Wright, A. Galerie, D. Monceau, S. Mathieu (Eds.), High Temperature Corrosion and Protection of Materials 7, Pts 1 and 2, Trans Tech Publications Ltd, 2008, pp. 463–472 595–598.
[38] C. Desgranges, F. Lequien, E. Aublant, M. Nastar, D. Monceau, Oxid. Met. 79 (2013) 93–105.
[39] Y. Adda, J. Philibert, La Diffusion dans les solides Bibliothèque Des Sciences Et Techniques Nucléaires, Institut National Des Sciences Et Techniques Nucléaires & Presses Universitaires De France, Paris, 1966.
[40] C. Wagner, Zeitshrift für Physik B21 (25) (1933).
[41] I. Kaur, Y. Mishin, W. Gust, Fundamentals of Grain and Interphase Boundary Diffusion, John Wiley, 1995.
[42] L.G. Harrison, Trans. Faraday Soc. 57 (1961) 1191–1199.
[43] D. Monceau, B. Pieraggi, Oxid. Met. 50 (1998) 477–493.
[44] B. Pieraggi, Oxid. Met. 27 (1987) 177–185.
[45] A. Atkinson, R.I. Taylor, A.E. Hugues, Philos. Mag. A 45 (5) (1982) 823–833.
[46] J. Zurek, D.J. Young, E. Essuman, M. Hänsel, H.J. Penkalla, L. Niewolak, W.J. Quadakkers, Mater. Sci. Eng. A 477 (2008) 259–270.
[47] D.J. Young, D. Naumenko, L. Niewolak, E. Wessel, L. Singheiser, W.J. Quadakkers, Mater. Corros. 61 (10) (2010) 838–844.
[48] L. Kjellqvist, M. Selleby, CALPHAD 33 (2009) 393–397.
[49] A.C.S. Sabioni, R.P.B. Ramos, V. Ji, F. Jomard, W.A.A. Macedo, P.L. Gastelois, V.B. Trindade, Oxid. Met. 78 (2012) 211–220.
[50] A. Atkinson, Oxid. Met. 28 (5/6) (1987) 353–389.